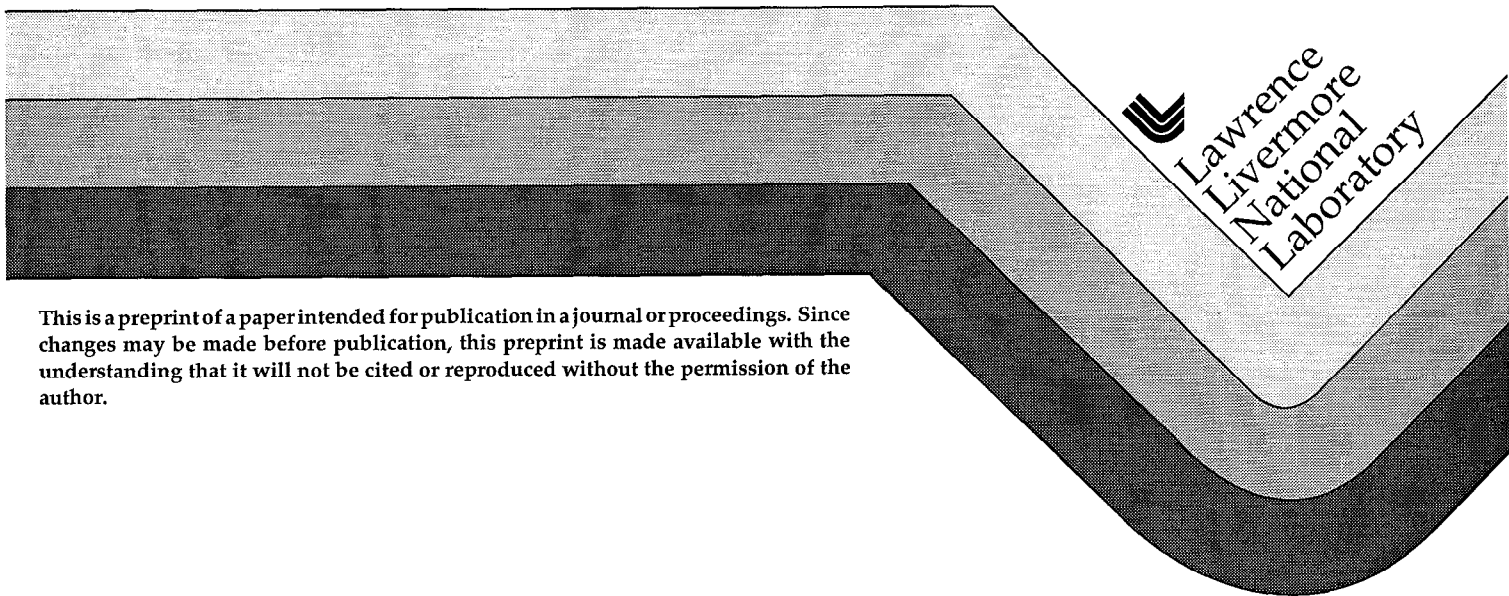


Drifts, Boundary Conditions and Convection on Open Field Lines

Ronald H. Cohen
Dmitri Ryutov

This paper was prepared for submittal to
40th Annual Meeting, American Physical Society, Division of Plasma Physics
New Orleans, LA
November 16-20, 1998

November 20, 1998



This is a preprint of a paper intended for publication in a journal or proceedings. Since changes may be made before publication, this preprint is made available with the understanding that it will not be cited or reproduced without the permission of the author.

DISCLAIMER

This document was prepared as an account of work sponsored by an agency of the United States Government. Neither the United States Government nor the University of California nor any of their employees, makes any warranty, express or implied, or assumes any legal liability or responsibility for the accuracy, completeness, or usefulness of any information, apparatus, product, or process disclosed, or represents that its use would not infringe privately owned rights. Reference herein to any specific commercial product, process, or service by trade name, trademark, manufacturer, or otherwise, does not necessarily constitute or imply its endorsement, recommendation, or favoring by the United States Government or the University of California. The views and opinions of authors expressed herein do not necessarily state or reflect those of the United States Government or the University of California, and shall not be used for advertising or product endorsement purposes.

Drifts, Boundary Conditions and Convection on Open Field Lines

Ronald H. Cohen, Dmitri Ryutov

Lawrence Livermore National Laboratory, P.O. Box 808, Livermore CA 94550

Abstract

In a number of plasmas of practical interest, including the scrape-off layer of a tokamak with a divertor or toroidal limiter, some gas discharge devices, and in the vicinity of spacecraft, magnetic field lines intersect bounding surfaces at shallow angles. Under these circumstances a number of interesting and important effects arise. Drifts can compete with parallel flows in establishing the boundary conditions for plasma mass-flow and current (sheath current-voltage characteristics). We derive the mass-flow constraints including both poloidal and radial drifts, review the current boundary conditions, and survey the consequences, including along-field density and heat-flux asymmetries, convection created by a wavy surface, generation of electric fields and surface currents associated with shadows from surface structures, and modification of instability growth rates.

I. INTRODUCTION

In magnetized plasmas, there is inevitably a region in which magnetic field lines are in contact with material walls. The properties of this interaction have profound consequences for the properties of the open-field line region, and this can in turn appreciably affect the behavior of the entire plasma. The plasma-wall interaction becomes particularly rich in the case of near-grazing incidence of magnetic field lines on walls, as then drifts can compete with parallel flows in their contribution to the mass and current flows to the walls. Near-grazing incidence occurs in the scrape-off layer of a tokamak with a divertor or toroidal limiter, some gas discharge devices, and in the vicinity of spacecraft.

Most of the relevant phenomena have been treated previously: the mass-flow boundary conditions without¹ and with² drifts, the current boundary conditions^{3,4}, the effects of drifts on asymmetries^{2,5-8}, induced convection⁹, surface structure irregularities^{10,11}, and the effect on instabilities¹²⁻¹⁹. The primary purpose of the present paper is to present a unified picture of these phenomena, clarifying their interactions. In the process, we add some new pieces to the picture, and clarify some misconceptions, apparent contradictions, and in some cases errors that have appeared in the earlier literature. The main new ingredients are a derivation of the mass-flow constraints (often mistaken for boundary conditions) that includes the effects of radial drifts and poloidal temperature and magnetic-field gradients, and a description of poloidal-drift-induced asymmetries that accounts for temperature and magnetic-field nonuniformities; these additions can substantially change, even reverse, the predicted asymmetries, and provides a picture in general agreement with experimental observations.

We consider a heated, magnetized device with a closed magnetic field lines or flux surfaces, surrounded by a region (the scrape-off layer, or SOL) where magnetic-field lines intersect walls. In order to have a specific reference point for nomenclature, we consider a toroidal magnetic-fusion device such as a tokamak (see Fig. 1), but the concepts apply to the other examples as well.

Rapid heat conduction along field lines to heat-absorbing physical or effective (e.g. dense neutral gas) walls leads to steep cross-field temperature gradients in the SOL, with a scale length smaller than that in the core plasma by order $(D_{\perp}/D_{\parallel})^{1/2}$ where D_{\perp} and D_{\parallel} are thermal diffusivities across and along field lines. In contrast to conditions in the core plasma, the potential in the SOL is set primarily by physics along magnetic field lines: the sheath potentials adjust to admit a current of the order of the ion saturation current or smaller to the walls, and the potential variation from the walls to the interior of the SOL is set by electron pressure balance. The net result is a mid-SOL potential Φ of order T_e/e , with a radial-gradient scale length L_{ϕ} comparable to the radial electron-temperature-gradient length λ_{Te} . This gives rise to a sizeable poloidal $\mathbf{E} \times \mathbf{B}$ drift velocity $v_{Ep} \sim \rho_s c_s / \lambda_{Te}$.

When magnetic field lines lie nearly in a symmetry direction (the toroidal direction, for a tokamak) and where field lines intersect walls which extend in this symmetry direction, then what is of interest is the projection of these flows into a plane perpendicular to the symmetry direction (the radial-poloidal plane) and we immediately see that the poloidal drifts can compete with parallel flows in establishing mass asymmetries, current and energy fluxes to the walls, etc, their ratio being of order $\rho_{pol} / \lambda_{Te}$ where ρ_{pol} is the gyroradius calculated using only the poloidal projection B_p of the magnetic field. Intuitively one might expect a poloidal drift to drive a density asymmetry with higher density in the direction pointed to by the drift, but we will see that, when account is taken of magnetic-field and temperature variations, the reverse can also happen. For a single-null-divertor tokamak, the “standard” direction of the magnetic field is the one in which the poloidal drifts in the SOL point to the outer divertor plate; experimentally, the higher density is often at the inner plate.

In addition to poloidal drifts, poloidal pressure variations (arising from momentum sinks and also magnetic-field variation) give rise to poloidal electric fields and hence radial drifts. Since the pressure is generally higher in the midst of the SOL than at either end, this drift changes sign over the length of a field line and contributes to asymmetry: the radial flux is inward over about half the flux surface and outward over the other, and is closed by a

return poloidal flux. Following Stangby and Chankin²⁰, we can estimate the importance of this term based on the return poloidal flux velocity it generates: $v_{p,ret} = \int dl_p d/dr (rv_{Er})$ where l_p denotes poloidal length. Since the electric drift is (apart from magnetic curvature) divergence-free, we can estimate v_{Er} to be $(L_r/L_p)v_{Ep}$, where L_r and L_p are poloidal and radial scale lengths; estimating $d/dr = 1/L_r$, we find $v_{p,ret} \sim v_{Ep}$, i.e. comparable radial and poloidal effects. We shall see in Sec. II that there are situations in which one or the other drift dominates.

When magnetic field lines intersect a bounding surface at a shallow angle, then we may expect the electric drift to play a significant role in establishing the mass flow conditions near the wall. It was pointed out in Ref. 2 that the mass flux at the wall is a property of the hydrodynamics equations and the degree of reflection at the wall, and has nothing to do with sheath dynamics, for example the condition^{21,22} of a monotonic laminar sheath. For the simple case of a uniform poloidal drift and an absorbing wall, analysis of the hydrodynamics continuity and momentum equations indicates² that $v_{||}\mathbf{b} \cdot \mathbf{e}_{pol} + \mathbf{v}_{Ep} = \pm c_s \mathbf{b} \cdot \mathbf{e}_{pol}$ at the bounding surface or, if one exists, at a “nozzle” upstream. (See sec. II for a definition of “nozzle”.) Here \mathbf{b} and \mathbf{e}_{pol} are unit vectors along the magnetic field and in the poloidal direction, and $c_s = [(T_e + T_i)/m_i]^{1/2}$ is the sound speed. Thus, the poloidal velocity at the critical point is the same as in the absence of the drifts, while the parallel velocity itself is altered. A more general case which includes radial drift and poloidally varying poloidal drift is considered in Sec. II; then, the critical poloidal velocity is itself altered from the case with no drift.

In addition to mass flow at the wall, the drifts can have a significant impact on the current-voltage characteristics of the sheath. In particular, contrary to common experience, the $\mathbf{E} \times \mathbf{B}$ drift leads to an ion current to the surface, as ions subjected to $\mathbf{E} \times \mathbf{B}$ drift can simply flow to the wall, whereas electrons are mostly repelled. The resulting sheath-voltage characteristics are then dependent on the angle of incidence of the field lines on the bounding surface.

There still remains misconceptions about the role of diamagnetic drifts in such consid-

erations. As pointed out in refs. 2 and 4, diamagnetic drifts result from motion of particles about stationary gyrocenters and so do not transport mass, momentum or heat. They do on the other hand represent a real current (which, however, is divergence-free, apart from curvature effects). Thus diamagnetic terms do not enter into the mass flow conditions, but do enter into the current boundary conditions, as will be seen in the next section.

The organization of the remainder of this paper is as follows: Section II contains a derivation of the hydrodynamic constraints on mass flows and the current boundary conditions. In section III we examine in detail the asymmetries produced by poloidal drifts, and also review the role of radial drifts. Section IV discusses several other consequences of the mass flow constraints and current boundary conditions, including the possibility of creating convection by making the bounding surfaces wavy, the phenomenology of shadows cast by surface structures, the generation of toroidal current, and effects on instabilities. Finally, Sec. V contains overall discussion and conclusions.

II. MASS FLOW CONSTRAINTS AND CURRENT BOUNDARY CONDITIONS

A. Mass flow

As noted above, the mass flow conditions follow from the hydrodynamics equations themselves, not from a sheath analysis. We confine ourselves exclusively to the case of axisymmetry. Then, taking into account that the $\mathbf{E} \times \mathbf{B}$ drift velocity is divergence-free, the continuity equation can be written in the form:

$$n \frac{\partial v_{\parallel}}{\partial s} + \hat{v}_{\parallel} \frac{\partial n}{\partial s} + v_r \frac{\partial n}{\partial r} = S_n + n v_{\parallel} \frac{\partial \ln B}{\partial s} \quad (1)$$

where v_r is the radial (normal to flux surface) $\mathbf{E} \times \mathbf{B}$ drift velocity, $\hat{v}_{\parallel} = v_{\parallel} + (B/B_p)v_{E_p}$, S_n is the particle source, and B_p is the poloidal magnetic field component. We consider B_p/B small and so neglect the distinction between B and the toroidal field B .

The radial drift v_r depends on the poloidal (or equivalently, the parallel) derivative of the potential ϕ , which we eliminate in favor of the parallel derivative of the electron

pressure p_e and the thermal force, neglecting the ohmic contribution to the electron parallel momentum equation (a good approximation for a tokamak SOL.) This allows us to re-write the continuity equation as:

$$n \frac{\partial v_{\parallel}}{\partial s} + \hat{v}_{\parallel} \frac{\partial n}{\partial s} + \frac{c}{eB_p \lambda_n} \left(\frac{\partial p_e}{\partial s} - 0.71 T_e \frac{\partial n}{\partial s} \right) = S_n + n v_{\parallel} \frac{\partial \ln B}{\partial s} \quad (2)$$

where $\lambda_n \equiv n(dn/dr)^{-1}$. Note that this expression applies for an arbitrary radial density variation and parallel electron pressure variation.

In a similar fashion we can write the plasma parallel momentum equation,

$$mn \hat{v}_{\parallel} \frac{\partial v_{\parallel}}{\partial s} = \frac{\partial p}{\partial s} - \frac{v_{\parallel}}{\omega_{cip} \lambda_v} \left(\frac{\partial p_e}{\partial s} - 0.71 T_e \frac{\partial n}{\partial s} \right) + S_v \quad (3)$$

where $p = p_e + p_i$ is the total pressure, $\lambda_v \equiv v_{\parallel}(dv_{\parallel}/dr)^{-1}$, and ω_{cip} is the ion cyclotron frequency in the poloidal field, eB_p/mc . We note that, in this non-conservation form, the velocity source S_v is $-nv_{\parallel}S_n$ plus the physical momentum density source (for example, charge exchange on cold neutrals).

Finally we close the system with a model for the electron and ion pressures. For simplicity we assume that the effective charge $Z_{eff} \approx 1$ so that we can neglect the distinction between the electron and ion densities, and we assume that p_e is proportional to the total pressure p (the ratio is 1/2 in the limit of high electron-ion collisionality). Then we consider two models: (1) isothermality along magnetic field lines, $\partial p/\partial s = T \partial n/\partial s$; and (2) a model in which the heat flux along field lines is flux-limited and its parallel derivative balances an explicit heat sink term (the sum of radiation, charge exchange, and radial losses):

$$Q + (\partial/\partial s)(\eta n T_e c_s) = 0 \quad (4)$$

where S_h is the explicit (negative) energy sink term and η is a constant of order 10. The isothermal model is relevant to a moderate-recycling attached divertor; the flux-limited model is applicable to the divertor leg of a present-day device in a high-recycling regime.

We proceed by eliminating $\partial p/\partial s$ and $\partial n/\partial s$ from Eq. (3) using Eq. (2) and one or the other pressure model. For the isothermal model, this gives:

$$\hat{v}_{\parallel} \left(1 - \frac{c_s \hat{c}_s}{\hat{v} \hat{v}_{\parallel}} \right) \frac{\partial v_{\parallel}}{\partial s} = - \frac{c_s \hat{c}_s}{\hat{v}} \left(\frac{S_n}{n} + v_{\parallel} \frac{\partial \ln B}{\partial s} \right) + \frac{S_v}{nm} \quad , \quad (5)$$

where $\hat{v} = \hat{v}_{\parallel} + c_{se} \rho_{se,p} / \lambda_n$, $\hat{c}_s = c_s + \rho_{se,p} v_{\parallel} / \lambda_v$, $c_{se} = (T_e / m_i)^{1/2}$, $c_s = [(T_e + T_i) / m_i]^{1/2}$, and $\rho_{se,p} = c_{se} / \omega_{cip}$.

For the flux-limited model, we obtain, from Eq. (4), the relation

$$\frac{\partial p}{\partial s} = \frac{1}{3} \frac{p}{n} \frac{\partial n}{\partial s} + \frac{2}{3} p \frac{\partial \ln B}{\partial s} + \frac{2}{3} \frac{S_h}{\eta c_s} \quad (6)$$

and then, from Eqs. (2), (3) and (6), we obtain

$$\hat{v}_{\parallel} \left(1 - \frac{1}{3} \frac{c_s^2 \epsilon_1}{\hat{v}_{\parallel} \hat{v}_{fl}} \right) \frac{\partial v_{\parallel}}{\partial s} = - \left[\frac{S_h \epsilon_2}{\eta n m c_s} + \frac{c_s^2 S_n}{3 n \hat{v}_{fl}} + c_s^2 \left(\frac{2}{3} + \frac{\epsilon_2 v_{\parallel}}{3 \hat{v}_{fl}} \right) \frac{\partial \ln B}{\partial s} \right] + \frac{S_v}{m n} \quad (7)$$

where $\hat{v}_{fl} = \hat{v}_{\parallel} - 0.14 \rho_{pe} c_{se} / \lambda_n$, $\epsilon_1 = 1 - 0.42 v_{\parallel} p_e / \omega_{cip} \lambda_v p$, and $\epsilon_2 = (2/3)(1 + 1.71 v_{\parallel} p_e / \omega_{cip} \lambda_v p) - 0.38 \epsilon_1 \rho_{pe} c_{se} / \lambda_n \hat{v}_{fl}$, and $\epsilon_2 = \epsilon_1 (1 - 1.14 \rho_{pe} c_{se} / \lambda_n v_{\parallel})$.

A third model that can straightforwardly be done is one where the divergence of the heat flux balances classical sources and sinks, but the flux is collisional heat diffusion. The result is identical to Eq. (5), but with additional (integrated in s) source terms on the right-hand side.

Equations (5) and (7) have the same structure, namely, a coefficient times $\partial v_{\parallel} / \partial s$ equals an effective source (physical sources plus a logarithmic derivative of the field strength). We consider the case of an absorbing wall (recycling is included in the sources). This is equivalent to extending the domain infinitely beyond the wall, with no sources and a decaying field strength. The outflow solution is one in which v_{\parallel} continuously increases (for increasing s) in this region as B decreases and a flux bundle expands. In order for this to happen, the coefficient of $\partial v_{\parallel} / \partial s$ must therefore be positive in this region, and thus zero or positive at the boundary. For isothermality and no drifts ($\hat{v}_{\parallel} \rightarrow v_{\parallel}$, $\lambda_n, \lambda_v \rightarrow \infty$) this is the familiar ‘‘Bohm’’ inequality (but unrelated in its origins to sheath physics): $v_{\parallel} \geq c_s$ at the wall. Considering poloidal, but not radial, drifts (which applies in the limit that λ_n and λ_v are large compared to the electron temperature scale length and hence the potential radial scale length), the condition becomes $\hat{v}_{\parallel} \geq c_s$, i.e. the poloidal velocity (projections of parallel and

$\mathbf{E} \times \mathbf{B}$ flow) equal or exceed the poloidal projection of sonic parallel flow. For the flux-limited model, c_s is replaced by $c_s/3^{1/2}$ (which is the speed of sound waves in such a medium). With the radial drift terms included, the condition is more complicated but is still supersonic-like.

Somewhere upstream, $\hat{v}_{\parallel} = 0$. (For the flux-limit model, this may occur inside the heat source region where the model doesn't apply, but typically \hat{v}_{\parallel} will be sub-sonic somewhere in the region of applicability). Hence, at the wall or somewhere upstream, there must be at least one place where the coefficient of $\partial v_{\parallel}/\partial s$ vanishes, *i.e.*, a sonic-supersonic transition. This must occur at a location where the right-hand side of Eq. (5) or (7) vanishes; more specifically, at a region where the effective source transitions from being positive downstream to negative further up. In a source-free region this can occur at a magnetic-field maximum, *i.e.*, at a magnetic nozzle, where the area of a flux bundle has a local minimum. More generally the presence of sources displaces the effective nozzle. (Interestingly, in a tokamak divertor leg there may be regions of both positive and negative S_n corresponding to ionization and recombination; the region in between may be the effective nozzle.)

What, then, constitutes an appropriate boundary condition for a fluid code? The continuity and momentum equations are a pair of first-order equations, and hence we need to specify two boundary conditions, total, on n and v_{\parallel} . A suitable pair is v_{\parallel} at both ends of the field line. Mathematically, there is a range of allowed subsonic choices, but the only sonic/supersonic choice allowed, and the only choice overall corresponding to absorbing walls, is values that produce a sub- to supersonic transition at an effective nozzle.

B. Current-voltage characteristics

The current at the plasma boundary has contributions from both parallel and drift components. The problem without drift components was treated by Chodurachordura. For small angles of incidence, the drift components are significant^{4,24}. The role of electrons and ions is very different, owing to the presence of the sheath which confines the electrons. (We assume that the angle of incidence is not so small [$< (m_e/m_i)^{1/2}$] that the ions become the

electrostatically confined species.) We review here the treatment presented in Ref. 24. The geometry is indicated in Fig. 2

Since the sheath pushes ions which approach it toward the wall, the poloidal projection of the ion current on the plasma side of the sheath is simply

$$j_{ni}^{(p)} = \alpha ne v_{\parallel} + \hat{\alpha} (j_{E_p} + j_{d_{pi}}) \quad (8)$$

where j_{E_p} and $j_{d_{pi}}$ are the poloidal components of the ion $\mathbf{E} \times \mathbf{B}$ and diamagnetic currents, respectively: $j_{E_p} = (cne/B)\partial\phi/\partial r$, $j_{d_{pi}} = (c/B)\partial p_i/\partial r$, α is the sine of the angle between the field line and the bounding surface (divertor plate, etc.), and $\hat{\alpha}$ is cosine of the same angle. If the bounding surface is toroidally symmetric, then α is just B_p/B . The ion current on the wall side of the sheath is different, because radially varying radial surface currents flow in the sheath region. These arise⁴ from radial $\mathbf{E} \times \mathbf{B}$ drift of ions while traversing the sheath and from uncompensated ion gyro-motion current (uncompensated because of the scrape-off of ions with gyro orbits that touch the wall). We can calculate the ion sheath current as follows: The momentum balance condition is, without approximation,

$$0 = -\frac{\partial \pi_{yy}^{(i)}}{\partial y} - en \frac{\partial \phi}{\partial y} - j_{ri} B \quad (9)$$

where y is the direction normal to the wall, and $\pi_{yy}^{(i)} \equiv m_i n_i \langle v_y^2 \rangle$. For the small angles of incidence under consideration, most of the sheath potential drop occurs in a quasineutral region with thickness of order of the ion gyroradius, rather than the non-neutral Debye sheath immediately adjacent to the wall. Within the quasineutral region electrons are strongly magnetized, so that the electron stress tensor can be characterized by just two pressure components $p_{\perp e}$ and $p_{\parallel e}$, and the parallel electron momentum equation implies that $en\partial\phi/\partial y = \partial p_{\parallel e}/\partial y$. With this substitution Eq. 9 can be integrated. We then note that on the plasma side of the sheath, $\pi_{yy}^{(i)} \approx p_{\perp i}$, while on the wall side, it is much smaller (by $\mathcal{O}(\alpha)$) because of ion scrape-off. Hence we obtain:

$$I_{ri} = -c (p_{\perp i} + p_{\parallel e}) / B \quad (10)$$

where I_{ri} is the radial current per unit toroidal length, and the pressures are evaluated on the plasma side of the sheath. From current continuity, $-dI_{ri}/dr$ must equal the change in normal ion current from the plasma to the wall side of the sheath; hence the ion current density at the wall is:

$$j_{ni}^{(w)} = \alpha nev_{\parallel} + \frac{cen}{B} \frac{\partial \phi}{\partial r} - \frac{c}{B} \frac{\partial p_{\parallel e}}{\partial r} \quad (11)$$

where all quantities on the right-hand side are evaluated on the plasma side of the sheath.

We consider now the electrons. For the angles of field line incidence we are considering, drifts can compete with parallel acoustic flows projected on to the direction normal to the wall, but not with the projection of parallel electron thermal flow. The flux of electrons approaching the sheath is (to within corrections of order of the mass ratio) the same as in the absence of drifts (and also nearly equal to the flux leaving the sheath.) The flux to the wall is $\sim \exp(-e\phi_{sheath})/T_e \sim (m_e/m_i)$ times this value, and thus the electron current at the wall is just

$$j_{ne}^{(w)} = \alpha j_{e0} \quad (12)$$

where j_{e0} is the parallel electron current that would escape over the same height sheath for normal incidence; here $\alpha = B_p/B$. For Maxwellian electrons, $j_{e0} \approx (env_{te}/2\pi)^{1/2}$. To get the electron current on the plasma side of the sheath, we perform a calculation analogous to that which we did for the ions (Eq. 10) for the sheath surface current; we obtain $I_{re} = c(p_{\perp i} - p_{\parallel e})/B$, which is zero for an isotropic distribution. Hence, the electron current on the plasma side of the sheath is

$$j_{ne}^{(p)} = \alpha j_{e0} + \frac{c}{B} \frac{\partial (p_{\perp e} - p_{\parallel e})}{\partial r} \quad (13)$$

The current boundary condition on the plasma side of the sheath, obtained by summing Eqs. (8) and (13), is the one to be applied for fluid simulations of a divertor or as boundary conditions for a low-frequency instability calculation. The boundary condition on the wall, the sum of Eqs. (11) and (12), is useful for determining the floating potential of an insulated wall or the input to a flush-mounted probe.

In applying the current boundary conditions, the value of v_{\parallel} is provided from the mass-flow boundary condition discussed in the preceding sub-section.

III. ASYMMETRY PRODUCED BY POLOIDAL DRIFTS

We consider in this section the role of poloidal drifts in the creation of poloidal asymmetries. We depart from previous analyses (*e.g.*, Ref. 2) by allowing for poloidal variations of temperature and drift velocity, but we neglect radial drifts.

We consider the situation of strong recycling near the divertor plates. In this case, the overall density is rather high, and there exists significant temperature asymmetry between the inner and outer strike points, with the temperature higher at the outer point. This can be explained by the larger surface area and weaker magnetic field on the outer side of the tokamak²⁵, together with a relatively low electron parallel thermal diffusivity at higher densities. The particle sources in this case are situated near the divertor plates, *i.e.*, near the points A and B in Fig. 1 To model the temperature variation, we assume that the temperature is equal to T_{out} in the outer divertor leg and main SOL, and is equal to $T_{in} < T_{out}$ near the source A and closer to the inner strike point. With equal source strengths, at high enough-temperature asymmetry the plasma density at the inner strike point will obviously be higher than at the outer strike point. But here we ask how the direction of the poloidal drift affects the asymmetry. At a large temperature difference, the particles from the hot outer region flow both to the outer and inner divertor plate (but with relatively few to the outer plate because of the higher mirror ratio and longer path length), with a sonic transition occurring at point 1 and at the outer wall. The particles born near the inner plate, at point B, experience therefore a pressure directed towards the inner divertor plate. This pressure is affected by the particle drift: if the drift is directed towards the outer divertor plate, this pressure is lower, whereas if the drift is directed towards the inner strike point, the pressure is higher. As the total number of particles produced by the source A is given, the higher pressure from the outside means a higher flow velocity at the divertor plate and,

accordingly, a lower density, in accord with the experimental trends.²⁶⁻²⁹ This example shows the richness of possible scenarios of hydrodynamic flows in the SOL and shows that the chains of causes and events can be quite subtle. In particular, the effect of the drifts on the density asymmetry contradicts the simple intuitive picture in which the asymmetry would follow direction of the particle drifts (weaker asymmetry for the normal direction of the magnetic field). In contrast, the private flux region has no magnetic nozzles and so no sonic transition between the sources; particles from both sources reach both plates, and the intuitive asymmetry should apply. Since the poloidal drift is opposite in the main SOL and private flux regions, both can contribute in the same direction to the asymmetry. in the direction observed experimentally.²⁶⁻²⁹

To be quantitative, we consider a simple model in which there are no radial drifts, and the drift velocity is constant. We also assume that the inner and outer strike points are situated in approximately the same magnetic field, i.e., the divertor legs are short. The solution for the density asymmetry is given parametrically, for supersonic transition at point 1, by

$$\frac{n_{in}}{n_{out}} = \frac{R + 2}{R} \frac{c_s^{out}}{M c_s^{in}} \quad ; \quad \frac{\hat{v}_E}{c_s^{out}} = \frac{R - (1 + R/2)(M + 1/M)c_s^{in}/c_s^{out}}{R + 1} \quad (14)$$

where R is the mirror ratio between the point 1 and the strike points and c_s^{out}/c_s^{in} is the ratio of sound speeds between the two strike points. Results are plotted in Fig. 3. The break in the curves corresponds to the situation where the sonic transition jumps from the inner strike point (to the right of the brake) to the throttle (point 1). One sees that, indeed, at high temperature ratio the change of the direction of the magnetic field from normal to reversed causes a decrease in the density asymmetry.

IV. OTHER CONSEQUENCES

It is evident that the sheath-voltage characteristics derived above have a dependence on the angle of incidence of the field lines on the bounding surfaces, *i.e.* the wall. Hence by varying this angle as a function of toroidal angle and radius, we can engineer corresponding

variations in the mid-SOL potential. In general the procedure to determine ϕ is to substitute the v_{\parallel} at either end consistent with the nozzle constraints derived in Sec. IIa into the current boundary conditions (13) at either end, and solve Ohm's law (the electron momentum equation) along the field line subject to these boundary conditions and consistent with the other fluid equations. If we consider an iterative (perturbative) solution, starting from the zero-order configuration of a straight uniform field, constant T_e and n_e and drifts, and no radial current transport, the exercise is particularly simple: The (zero-order) electric drift current is divergence-free, so the net current entering a flux bundle at one bounding surface (plasma side of sheath) must equal the current leaving at the other. From Eqs. (8) and (13) we obtain expressions for j_f , current per unit flux-tube area, at each end:

$$j_{f1,2} = en \left[\left(v_{\parallel 1,2} \mp v_{Ep} \exp(-e\phi_{1,2}/T) \right) + (v_E + v_d)/\alpha_{1,2} \right] \quad (15)$$

Substituting $v_{\parallel 1,2} = \pm c_s - \hat{v}_E$, setting $j_{f1} = j_{f2}$, and subtracting the equations for the two ends, we obtain that the perturbation in ϕ is given by

$$\exp(-e\Delta\phi/T_e) \sim \frac{v_{Ep} + v_{di}}{2c_s} \left(\frac{1}{\alpha_2} - \frac{1}{\alpha_1} \right) \quad (16)$$

and we see that it is not difficult to get ϕ perturbations of order T_e .

This observation opens the possibility of deliberately introducing toroidal (and probably also radial) ripples on the surface, with the goal of inducing convection⁹ to stir the SOL and broaden the heat load on the bounding surfaces. (Such stirring might also be useful for increasing the uniformity in magnetized plasma processing devices.) Surface ripple is one of several methods considered in Ref. 9 for creating toroidally varying potentials.

Another consequence of the physics leading to the modified sheath current-voltage characteristics comes from the fact that the reflection of electrons by the sheath has the effect of setting up parallel currents to close/compensate for the electron $\mathbf{E} \times \mathbf{B}$ and diamagnetic currents. Hence the inclination of the field lines relative to the walls serves as a source of toroidal current in the main SOL (even in the absence of any waviness).

For near-grazing incidence, it is easy for surface deformations to be high enough that

“shadows” form behind the deformations: field lines pass through a deformation and re-emerge on the other side. Such deformations occur naturally on some scale. While the details depend on the relative scales of the surface deformations and the electron and ion gyroradii, in all cases the area “wetted” by plasma coming from the main volume becomes a small fraction of the total surface area, which has implications for sputtering. But another interesting phenomenon is that, for surface features of the order of the ion gyroradius or smaller, the wetted areas and shadows are different for ions and electrons, leading to charging of the surface and the shadows, trapping of cold, locally produced electron populations in the ion shadows, and potential structures that extend back into the SOL plasma and can produce convection cells with dimensions comparable to the surface deformation size.

Finally, there are a number of ways in which drifts have an impact on instabilities in the SOL. There are two classes of instabilities which owe their existence to the presence of the sheath: in one^{12,13}, the $\mathbf{E} \times \mathbf{B}$ -induced rotation of the plasma relative to the conducting wall leads to a negative sheath impedance which produces a drift-type instability. In another^{14,16}, the combination of sheath impedance and parallel variation of the $\mathbf{E} \times \mathbf{B}$ rotation rate drives Alfvén waves. The presence of the drift terms in the boundary conditions (8) and (13) changes the symmetry of the modes and can produce significantly increased growth rates¹⁹.

For higher-frequency modes ($\omega \sim c_s/\rho_p$) there are corrections to the current boundary conditions arising from transient charging of the sheath boundary layer¹⁷. Finally, the presence of a gyroradius-scale sheath with beam-like ion distribution functions allows for the possibility of microinstabilities within the sheath¹⁸.

V. DISCUSSION AND CONCLUSIONS

The question of the appropriate boundary conditions to be applied in boundary-plasma fluid simulations is a recurring one. The discussion in Secs. I and II should make it clear that the conditions on mass and momentum do not arise from an analysis of sheath physics, but rather from the hydrodynamics equations themselves, coupled with a statement that

the bounding surfaces are, for example, completely absorbing. One is naturally led to ask what would happen if the hydrodynamics equations yield a velocity at the wall below that for a laminar, quiescent sheath (as can happen for our flux-limited model). The answer is that the sheath has to adjust to accommodate the flow. This might be accomplished by the development of turbulence within the sheath.

We have also seen that, in the absence of viscosity, the momentum and continuity equations combined require two boundary conditions, which logically are just the parallel velocities at either end which give a sub- to super-sonic transition at an effective “nozzle”, at which the sum of $d(\ln B)/ds$ plus sources vanishes. The proper “boundary” conditions are then often not to be applied at the boundary: one should identify the nozzle locations and apply the supersonic transition criterion there. In the paper, we derived the appropriate criteria, including the effects of radial as well as poloidal drifts, for several different pressure-variation prescriptions. We note that the relative importance of radial and poloidal drift effects scales roughly as the ratio of radial scale lengths $\lambda_{Te}/\min(\lambda_n, \lambda_v)$.

As shown in Sec. III, the supersonic transition requirements coupled with a temperature asymmetry can lead to the counter-intuitive result of the poloidal drifts raising (lowering) the density near the wall that the drifts point away from (towards), while continuing to drive particle and heat flux in the direction of the drift. This results from the interplay of drift and parallel flows dictated by the supersonic transition requirements. In the context of a tokamak SOL this will enhance density and temperature asymmetries in the direction observed in experiments. The private flux region, because of its weaker sources, shorter length, and different magnetic-nozzle structure, may behave in the more intuitive direction; this remains to be explored.

A shallow angle of incidence of field lines on walls (or on an effective wall of neutral gas, in the case of an electrically detached plasma) has a significant impact on the sheath current-voltage characteristics when drifts are included. In particular, the ion $\mathbf{E} \times \mathbf{B}$ and diamagnetic currents are part of the current flow to the wall. These results have a number of consequences: (1) Convection can be deliberately created by making the bounding surfaces “wavy” in the

toroidal and radial directions. (2) If these or other-scale surface deformations are sufficiently steep, they form shadows in the magnetic field. The result is that only a fraction of the surface is wetted by the upstream plasma, and because the wetted areas for electrons and ions differ, pieces of the surface tend to charge up, driving surface currents, and the plasma acquires cross-field electric fields with scales dictated by the surface irregularity scales. (3) Instabilities: the modified boundary conditions can alter the structure and increase the growth rate of low-frequency sheath-driven modes; higher-frequency modes can be affected by transient charging of the gyroradius-scale sheath; and modes internal to the sheath can be driven by the beam-like distribution of ions there.

VI. ACKNOWLEDGMENTS

We thank Tom Rognlien for valuable discussions. This work was performed under the auspices of the U.S. Department of Energy by Lawrence Livermore National Laboratory under contract W7405-ENG-48.

REFERENCES

- ¹ P. J. Harbour, A. Loarte, *Contrib. Plasma Phys.* **34**, 312 (1994).
- ² R. H. Cohen and D. D. Ryutov, *Comments Plasma Phys. Controlled Fusion* **16**, 255 (1995).
- ³ A. V. Chankin and P. C. Stangby, *Plasma Phys. Controlled Fusion* **36**, 1485 (1994).
- ⁴ R. H. Cohen and D. D. Ryutov, *Phys. Plasmas* **2**, 2019 (1995).
- ⁵ F.L. Hinton, G.M. Staebler, *Nucl. Fusion* **29**, 405 (1989).
- ⁶ M. Tendler, V. Rozhansky. *Comm. on Plasma Phys and Contr. Fus.*, **13**, 191 (1991).
- ⁷ S.I. Krasheninnikov, P. Yushmanov and D. Sigmar, *Phys. Plasmas*, v. 2, 1972 (1995).
- ⁸ A. V. Chankin, *J. Nucl. Materials* **241-243**, 199 (1996).
- ⁹ R. H. Cohen and D. D. Ryutov, *Nucl. Fusion* **37**, 621 (1997).
- ¹⁰ R. H. Cohen and D. D. Ryutov, *Phys. Plasmas* **5**, 2194 (1998).
- ¹¹ R. H. Cohen and D. D. Ryutov, *J. Nucl. Materials*, in press.
- ¹² H. L. Berk, D. D. Ryutov, and Yu Tsidulko, *Phys. Fluids B* **3**, 1346 (1991)
- ¹³ H. L. Berk, R. H. Cohen, D. D. Ryutov, Yu Tsidulko and X. Q. Xu, *Nucl. Fusion* **33**, 263 (1993).
- ¹⁴ Yu Tsidulko, H. L. Berk and R. H. Cohen, *Phys. Plasmas* **1**, 1199 (1994).
- ¹⁵ R. H. Cohen, N. Mattor and X. Q. Xu, *Contrib. Plasma Phys.* **34**, 232 (1994), and references therein
- ¹⁶ J. R. Myra, D. A. Dippolito and J. P. Goedboed, *Phys. Plasmas* **4**, 1997.
- ¹⁷ R. H. Cohen and D. D. Ryutov, *Fizika Plazmy* **23**, 872 (1997) [*Plasma Phys. Reports* **23**, 805 (1997)].

- ¹⁸ R. H. Cohen and D. D. Ryutov, *Phys. Plasmas* **4**, 905 (1997).
- ¹⁹ B. C. Modi, X. Q. Xu, R. H. Cohen, and T. K. Fowler, *Bull. Am. Phys. Soc.* **40**, 1883 (1995).
- ²⁰ P. C. Stangby and A. V. Chankin, *Nucl. Fusion* **36**, 839 (1996).
- ²¹ K.-U. Riemann, *J. Phys. D: Appl. Phys.*, **24**, 493 (1991).
- ²² P.C. Stangeby, A.V. Chankin. *Phys. Plasmas*, **2**, 707 (1995)
- ²³ R. Chodura, *Phys. Fluids* **25**, 1628 (1982)
- ²⁴ D.D. Ryutov, *Contrib. Plasma Phys.* **36**, 207 (1996).
- ²⁵ P. J. Harbour, *Contrib. Plasma Phys.* **28**, 417 (1988)
- ²⁶ D.N. Hill, *et al.* *J. Nucl. Mater.*, **176-177**, 158 (1990).
- ²⁷ K. Itami, M. Shimada, N. Hosogane. *J. Nucl. Mater.* **196-198**, 755 (1992).
- ²⁸ A. Herrmann et al., *Plasma Phys and Contr. Fusion*, **37**, 17 (1995).
- ²⁹ S. Allen et al. Paper IAEA-F1-CN-69/EXP6/6 presented at 17th IAEA Fusion Energy Conference, Yokohama, Japan, 1998.

FIGURES

FIG. 1. Poloidal cross section of a tokamak, showing SOL and locations of field maxima (numbers) and sources (letters) discussed in text

FIG. 2. Schematic representation of a field line intersecting a divertor plate

FIG. 3. Density asymmetry vs. normalized drift velocity toward outer divertor plate

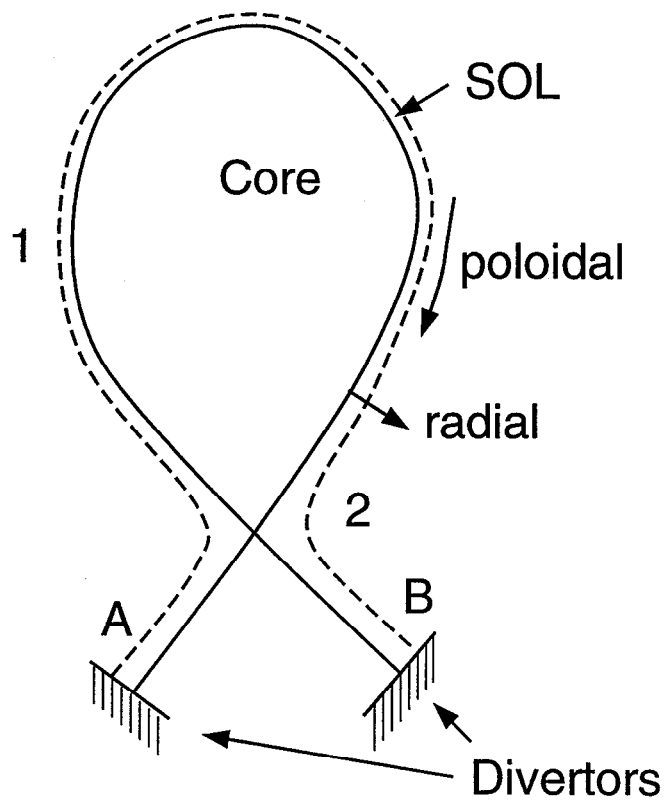


FIG 1

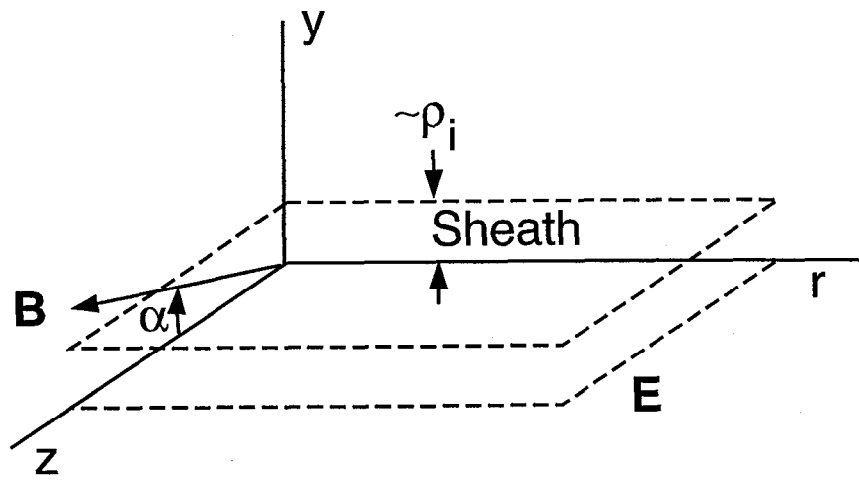


FIG 2

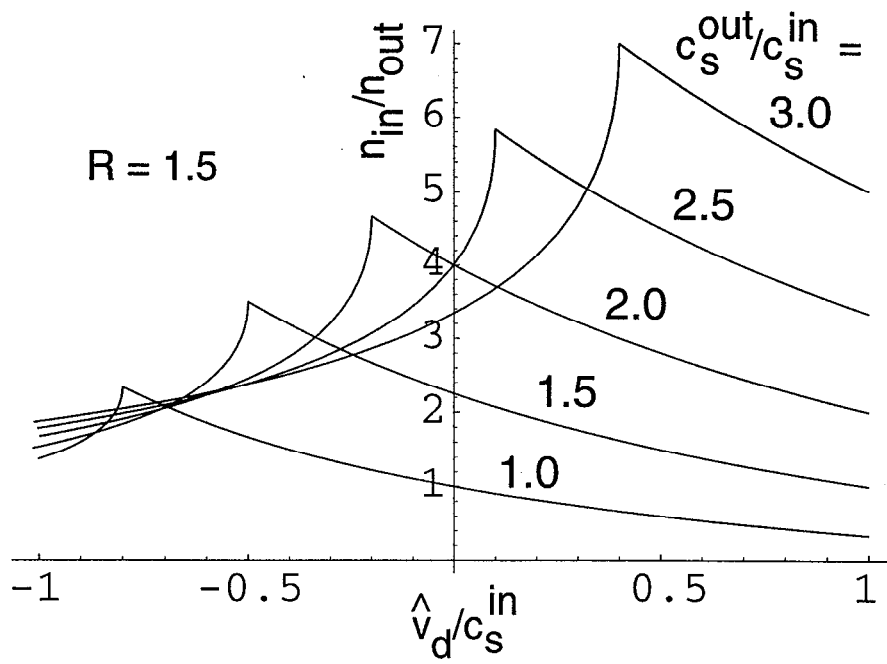


FIG 3